

Article

# UV-Curable Hydrophobic Coatings of Functionalized Carbon Microspheres with Good Mechanical Properties and Corrosion Resistance

Jiajia Wen <sup>1</sup>, Chengchen Feng <sup>1</sup>, Huijie Li <sup>1</sup>, Xinghai Liu <sup>1,\*</sup> , Fuyuan Ding <sup>1</sup>, Houbin Li <sup>1</sup> and Chi Huang <sup>2</sup>

<sup>1</sup> School of Printing and Packaging, Wuhan University, No. 299, Av. Bayi, Wuhan 430072, China; whu2018wenjiajia@163.com (J.W.); 2016301750075@whu.edu.cn (C.F.); huijie\_li01@sina.com (H.L.); dingfuyuan@whu.edu.cn (F.D.); lhb@whu.edu.cn (H.L.)

<sup>2</sup> College of Chemistry and Molecular Sciences, Wuhan University, No. 299, Av. Bayi, Wuhan 430072, China; chihuang@whu.edu.cn

\* Correspondence: liuxh@whu.edu.cn; Tel.: +86-27-6877-8489

Received: 16 October 2018; Accepted: 24 November 2018; Published: 29 November 2018



**Abstract:** Polyurethane acrylates (PUAs) are a kind of UV curable prepolymer with excellent comprehensive performance. However, PUAs are highly hydrophilic and when applied outdoors, presenting serious problems caused by rain such as discoloring, losing luster and blistering. Thus, it's important to improve their hydrophobicity and resistance against corrosion. In this paper, carbon microspheres (CMSs) were modified through chemical grafting method. Active double bonds were introduced onto the surface of organic carbon microspheres (OCMSs) and the functional product was referred to as FCMS. The results of Transmission Electron Microscope (TEM), X-ray Photoelectron Spectroscopy (XPS) and Thermogravimetric analysis (TGA) showed that organic chain segments were successfully connected to the surface of OCMSs and the grafting efficiency was as high as 16%. FCMSs were successfully added into UV-curable polyurethane acrylate prepolymer to achieve a hydrophobic coating layer with good mechanical properties, thermal stability and corrosion resistance. When the addition of FCMSs were 1%, thermogravimetric analysis (TGA) results showed that 5% of the initial mass was lost at 297 °C. The water absorption decreased from 52% to 38% and the water contact angle of the PUA composite increased from 72° to 106°. The pencil hardness increased to 4H and obvious crack termination phenomenon was observed in SEM images. Moreover, the corrosion rate was decreased from 0.124 to 0.076 mm/a.

**Keywords:** polyurethane; carbon microspheres; UV; glucose hydrothermal method; organic functional modification; hydrophobic

## 1. Introduction

With the developments of science technology and economy, people's demands for environment-friendly coatings are getting higher. UV curing coating is a new type of coating which is popular in Europe, America, and Japan in the late 20th century. UV coatings were first applied to the surface coating of furniture and flooring. And its application areas are further expanded to the field of household appliances such as cosmetic containers, televisions and computers. Compared with traditional coatings, UV curing coatings have developed rapidly in recent years due to their excellent economic benefits and environmental performance [1,2]. In 2010, the global UV curing coating market was about \$35.65 billion, which will reach \$75.90 million in 2019. Polyurethane acrylates (PUAs) are a kind of UV curable prepolymer with excellent comprehensive performances

such as excellent flexibility, low temperature resistance, frictional resistance, excellent weatherability, and optical property [1–4]. They are widely used in UV-curable coatings, inks, and adhesives. In the past two years, more and more manufacturers have tried to use PUAs. This will be the future trend of development. However, PUAs are highly hydrophilic and can easily lose their lustre and blister in high humidity and temperature. To solve these problems, it is necessary to improve the hydrophobicity and corrosion resistance of PUA coatings.

To improve the corrosion resistance of PUA coatings, it is necessary to reduce the water absorption and water permeability, as well as to improve the mechanical strength and adhesion on the substrate. Nowadays adding moderate nanoparticle fillers such as clay, SiO<sub>2</sub>, TiO<sub>2</sub>, ZnO, Al<sub>2</sub>O<sub>3</sub>, and Fe<sub>2</sub>O<sub>3</sub> into organic coatings can improve the coatings' corrosion resistance which has been identified as an effective way [5–11]. These nanoparticles can effectively reduce thermal stress and shrinkage stress during curing the process.

CMSs have excellent performances and unique structures such as large specific surface areas, low density, chemical stability, good electrical conductivity and thermal conductivity and so on [12]. Many methods have been used to prepare carbon microspheres such as chemical vapor deposition [13], spray drying [14], and hydrothermal method [15–17]. As the hydrothermal method has advantages including easy operation, relatively high purity product and low production cost, it has been the main method to prepare CMSs [12,18–20]. Glucose [21] is widely used as a main raw material for preparing CMSs through hydrothermal method. The surface of CMSs prepared by hydrothermal method contains many functional groups, such as hydroxyl and carbonyl groups [15]. CMSs have poor dispersity in organic solvents or organic composites, and there are strong van der Waals forces and little active sites on its surface. Thus, the application of CMSs was limited in different kinds of materials. The specific chemical modification would introduce some functional groups onto its surface and expand its application range.

In this paper, OCMSs were obtained by surface oxidation of CMSs which were prepared by hydrothermal method. Subsequently, the condensation reaction of toluene-2,4-diisocyanate (TDI) against the active hydroxyl groups on the surface of OCMSs was carried out, followed by capping with hydroxyethyl acrylate (HEA) to achieve FCMSs. Through this method, UV active double bonds were successfully introduced into OCMSs. FTIR, TEM and XPS were used to analyse the surface composition and morphology of carbon microspheres before and after surface organic grafting modification. The dispersion of carbon microspheres in acetone and acid–base solution was also studied. Finally, FCMSs were successfully applied to UV-curable PUA coatings to improve the thermal stability, mechanical property and corrosion resistance. This hydrophobic coating layer has good mechanical properties, thermal stability and corrosion resistance. So, it can be used in natural wood or wooden furniture to produce high-gloss closed lines or sub-light patterns of the finishing effect. Due to its special properties, such as corrosion resistance and hydrophobicity, it can be used the primer coatings of vehicles and ships. To the best of our knowledge, it was the first time that FCMS had improved the corrosion of PUA.

## 2. Materials and Methods

### 2.1. Materials

Glucose, ethyl alcohol, concentrated sulfuric acid, concentrated nitric acid, acetone, toluene-2,4-diisocyanate (TDI), hydroquinone and trichloroethane were all purchased from Sinopharm Chemical Reagent Co., Ltd., Shanghai, China. 2-hydroxyethyl acrylate (HEA), dibutyltin dilaurate (DBTDL) and 1,6-hexanediol diacrylate (HDDA) were provided by Shanghai Aladdin Bio-Chem Technology Co., Ltd., Shanghai, China. TDI must be distilled by reduced pressure distillation. Carbon paper was purchased from Ai Zhi Electric Appliance Factory, Shanghai, China. All other chemicals, unless expressly mentioned, were used as received.

## 2.2. Preparation of Carbon Microspheres

The carbon microspheres were prepared according to the hydrothermal method by Sun et al. [15]. Firstly, 50 mL of deionized water was poured into a 100 mL beaker. Insert a stir bar and sit the beaker on a hot plate. Then measure out 9.00 g of glucose and add it to the beaker. Add more deionized water to bring the total volume up to 100 mL. Then the solution was ultrasonically dispersed for 5 min. After the glucose was completely dissolved, the solution was transferred to a 150 mL polytetrafluoroethylene reactor and reacted for 10 h at 190 °C. When the reaction kettle was naturally cool, pour out the brown product of the reaction kettle, then repeated centrifugation, washing and ultrasonic process multiple times with deionized water and ethanol. Finally, the brown product was dried in a freeze dryer for 24 h to obtain brown CMSs.

2.00 g CMSs, 90 mL concentrated sulfuric acid and 30 mL concentrated nitric acid were put into the three-necked flask equipped with a thermometer and a condensate return tube. To make CMSs disperse evenly, the solution was put into ultrasonic apparatus for 20 min at room temperature. Then the mixture was magnetically stirred in an oil bath at 90 °C for 5 h. When the mixture was cool, it was washed with deionized water to get neutral mixture, and the final product was dried in a freeze dryer for 24 h to get light brown oxidation CMSs (OCMSs).

## 2.3. Organic Modification of OCMSs

0.60 g OCMSs were put in acetone solution and ultrasonically dispersed for 20 min to gain a homogeneous suspension. Then the suspension was poured into a 250 mL three-necked flask equipped with a condensate reflux tube and a constant pressure dropping funnel. 10 mL acetone, 8.71g TDI and 0.20 g DBTDL were added to the constant pressure dropping funnel. And the mixed liquor was slowly added into the flask at 70 °C. After reacting for 3 h, the system was cooled to 50 °C. 0.10 g hydroquinone was added into the flask and a mixture of 12.19 g HEA and 10 mL acetone were added dropwise to the system. After 12 h, the reaction system was cooled to room temperature. The suspension was washed by chloroform for several times and was centrifuged twice by deionized water in the end. The product was dried in a freeze-drying agent for 24 h to get FCMSs. The graft reaction process of OCMSs was shown in Figure 1 (Schematic illustration of the synthesis procedures of FCMSs and UV curing procedure of hydrophobic coatings of functionalized carbon microspheres). In this experiment, the grafting rate was controlled by the concentration of reactants TDI and HEA, and the surface grafting rate of OCMSs was obtained by TGA and XPS.

## 2.4. Preparation of UV-Curable Coatings

PUA prepolymer was prepared by the method in previous articles [22–25]. PUA prepolymer and HDDA active diluent were mixed at a ratio of 8:2, adding appropriate amount of ethanol and 2 wt % TPO. Different contents of FCMSs (0 wt %, 0.1 wt %, 0.5 wt % and 1.0 wt %) or 1.0 wt % OCMSs was added into the coating system. They were recorded as PUA, PUA/FCMSs-1, PUA/FCMSs-2, PUA/FCMSs-3, PUA/OCMSs, respectively. After the above mixture was ultrasonicated for 20 min, the homogeneous mixture was placed in a fuming cupboard for 1h to remove the ethanol solvent from the system. The mixture was then poured into Teflon molds and cured in a UV curing machine to obtain UV-curable coatings. The coating thickness of PUA coating is 1 mm. At a mercury lamp with a power of 80 W cm<sup>-1</sup>, keep the distance at 80 mm for 30 s. Then we can get the cured PUA layer.

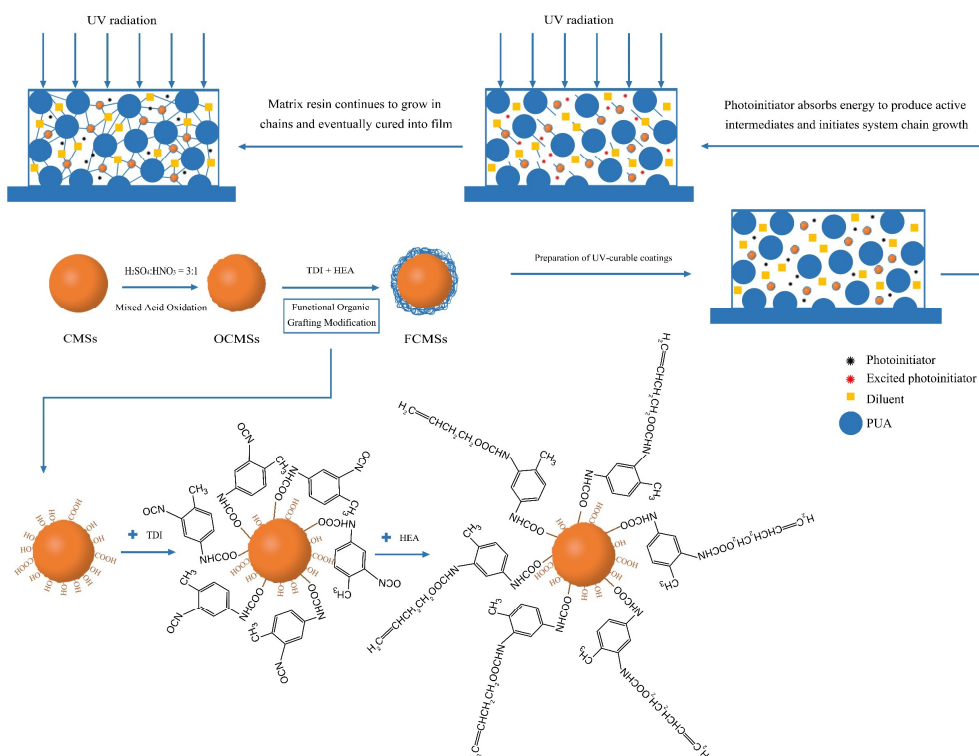


**Figure 1.** Schematic illustration of the synthesis procedures of functional coated microspheres (FCMs) and UV curing procedure of hydrophobic coatings of functionalized carbon microspheres.

2.5. Determination of Gel Rate of Cured Coatings

UV cured films were cut into a size of 20 mm × 20 mm × 1 mm and dried in a vacuum drying oven at 60 °C for 12 h. Subsequently, the films were placed in toluene solution and stored at room temperature for 48 h. Then the cured films were taken out and placed in a vacuum oven at 60 °C for 12 h. The gel ratio (GR) was calculated using Equation (1):

$$GR = (m_1 - m_0) / m_0 \times 100\% \tag{1}$$

where  $m_0$  and  $m_1$  were respectively the weight of films before and after swelling.

2.6. Determination of Water Absorption

UV cured films were cut into a size of 20 mm × 20 mm × 1 mm and were dried in the vacuum drying oven at 60 °C for 12 h. Subsequently, the films were placed in deionized water solution and stored in oven at 60 °C for 48 h. The water absorption rate (WR) was calculated using Equation (2).

$$WR = (m_3 - m_2) / m_2 \times 100\% \tag{2}$$

where  $m_2$  and  $m_3$  were respectively the weight of films before and after absorbing water.

2.7. Determination of Corrosion Resistance

The CV series electrochemical workstation of Wuhan Kester Instrument Co., Ltd. (Wuhan, China) was used to test corrosion resistance of the samples. There was a three-electrode system. The coating was coated on carbon paper, and the carbon paper was used as the working electrode (WE). The saturated calomel electrode was used as the reference electrode (RE), and the platinum electrode was used as the counter electrode (CE). The test area was 1.0 cm<sup>2</sup>.

## 2.8. Characterization

PUA, OCMSs and FCMSs were characterized using Fourier Transform Infrared Spectroscopy (FTIR) of Thermo Nicolet (Thermo Nicolet 5700, Waltham, MA, USA), and the scanning range was from 4000 to 400  $\text{cm}^{-1}$ . TGA was performed on a SETSYS-1750 type thermal analyzer of SETARAM with a scanning heating rate of 10  $^{\circ}\text{C min}^{-1}$  from ambient temperature to 1000  $^{\circ}\text{C}$  (Setaram, Lyon, France). XPS was carried out on ESCALAB250Xi X-ray electron spectrometer of Thermo Fisher Scientific (Thermo Scientific ESCALAB 250Xi, Waltham, MA, USA). X-ray diffraction (XRD) was characterized using a XPert Pro X-ray diffractometer of PAN analytical (PANalytical X'Pert Pro, Alemlo, Netherlands), and the scanning speed and range were 6  $^{\circ} \text{min}^{-1}$  and from 8  $^{\circ}$  to 80  $^{\circ}$ , respectively. Scanning electron microscopy (SEM) was tested using a SIGMA emission scanning electron microscope of Carl Zeiss (Hitachi S-4800, Tokyo, Japan). TEM was performed on a 1011 transmission electron microscope of JEM of Japan (JEM-2100, Japan Electronics Corporation, Akishima, Japan). UV-Vis absorption test (UV-Vis) was carried out by using 3600 UV visible near infrared spectrophotometer of Shimadzu. Pencil hardness was characterized using a pencil hardness tester of QHQ which was provided by Tianjin China vision technology development co. LTD, which was measured according to ASTM D3363 [26]. Water contact angle (WCA) was obtained by using an A10 dynamic/static surface/interface tension instrument (Kenuo Industries Ltd., Shanghai, China)

## 3. Results and Discussion

### 3.1. FTIR Results Analysis

The main structures of PUA, OCMSs and FCMSs were characterized via FTIR spectra, which were given in Figure 2. There are several characteristic peaks in the result of PUA. The peaks at 3513 and 3297  $\text{cm}^{-1}$  were ascribed to the stretching vibration of N–H which was highly sensitive to hydrogen bond distribution. The peaks at 1536  $\text{cm}^{-1}$  and 1732  $\text{cm}^{-1}$  were ascribed to the bending vibration of N–H and the stretching vibration O–C=O. These results showed carbamate bond (–NHCOO–) was formed by the reaction between –NCO and –OH. The peak at 1636  $\text{cm}^{-1}$  was the stretching vibration of the carbon-carbon double bonds (C=C) and the peak at 1410  $\text{cm}^{-1}$  belonged to the in-plane bending vibration of C–H on C=C bonds. The absorption peaks at 990 and 948  $\text{cm}^{-1}$  were assigned to the out-of-plane bending vibration of C–H on C=C bonds. These peaks indicated that HEA was successfully added to the PUA main chain. The peaks at 1602 and 811  $\text{cm}^{-1}$  were the benzene skeleton vibration and the out-of-plane bending vibration of C–H on benzene, respectively. The peak at 1076  $\text{cm}^{-1}$  was the stretching vibration of C–O–C which indicated that PEG was also added to the main chains of PUA. Furthermore, the FTIR curve did not have the characteristic peak of –NCO at 2270  $\text{cm}^{-1}$ , which illustrated that all –NCO groups reacted with –OH groups to form PUA.

There were also some characteristic peaks appeared in the result of OCMSs. The peak at 3435  $\text{cm}^{-1}$  corresponded to the hydroxyl group absorption peak on the surface of carbon microspheres. The two small peaks at 2970 and 2922  $\text{cm}^{-1}$  were the stretching vibration of C–H in the aliphatic section. The carbonyl (C=O) vibrational absorption peak shifted to 1705  $\text{cm}^{-1}$  and the hydroxyl peak was broadened, which indicated the presence of intramolecular hydrogen bonds. The presences of two peaks at 1507 and 1440  $\text{cm}^{-1}$ , respectively, were the vibration of the benzene ring skeleton. The peaks at 1023, 873 and 783  $\text{cm}^{-1}$  corresponded to the C–H out-of-plane bending vibration of the aromatic ring. These peaks indicated that the glucose had undergone a certain degree of aromatization in the hydrothermal environment. The peaks at 1382 and 1321  $\text{cm}^{-1}$  corresponded to the stretching vibration of C–O–C which may be an ether group or an ester group. In Figure 2, there were some new peaks in the spectra of FCMSs compared with OCMSs. The peak at 1714 and 1196  $\text{cm}^{-1}$  corresponded to the stretching vibration of C=O and C–O bond in the carbamate bond, respectively. The peaks at 1621 and 1543  $\text{cm}^{-1}$  were the stretching vibration and bending vibration peaks of the C–N bond in the carbamate bond, respectively. The stretching vibration peak of C=C double bond was at 1654  $\text{cm}^{-1}$  and there was a clear vibration peak of the benzene ring skeleton at 1437  $\text{cm}^{-1}$ . The presences of these

new peaks indicated that the PU structure (TDI-HEA) was successfully introduced onto the surface of OCMSs.

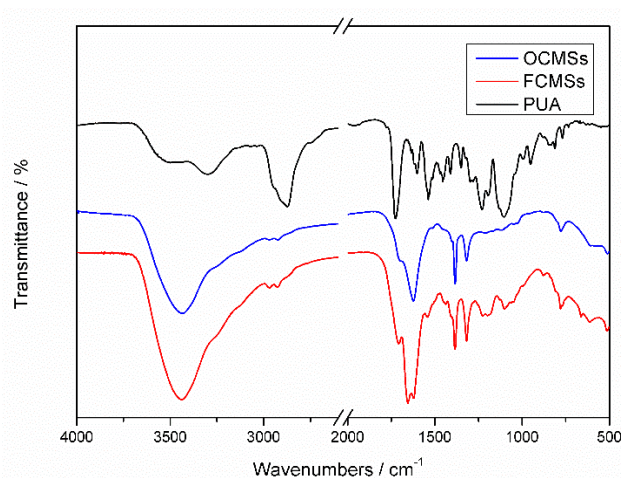


**Figure 2.** The FTIR spectra of polyurethane acrylates (PUA), organic carbon microspheres (OCMSs) and FCMSs.

### 3.2. Analysis and Results of TEM, XPS and TG of OCMSs and FCMSs

The TEM results of OCMSs and FCMSs were shown in Figure 3. As can be seen from the figures, the size of OCMSs and FCMSs was around 500 nm. Compared with the TEM diagram of OCMSs, the surface of FCMSs particles had a clear coating layer. The C, O and N elements were detected on the surface of FCMSs by photoelectron spectroscopy as shown in Figure 4a. The N1s peak appeared at the electron binding energy of 400 eV and the atom ratio of C, O and N were 69%, 14.53% and 16.47%, respectively. The formation of the C1s peak was shown in Figure 4b. In Figure 4b, the peaks at 289.06, 285.80 and 284.40 eV corresponded to O–C=O, C–O–C and C–C, respectively. These peaks showed the presence of characteristic structures of PU on the surface of FCMSs.

Figure 5 showed the TGA results of FCMSs and OCMSs. The thermal stability of FCMSs was lower than that of OCMSs. The weight loss of OCMSs in the range of 400 to 600 °C was obvious, while that was more obvious for FCMSs in the range of 100 to 400 °C. It also can be seen from the TG diagram that the high grafting rate of the PU structure on the surface of FCMSs was 16.7%.

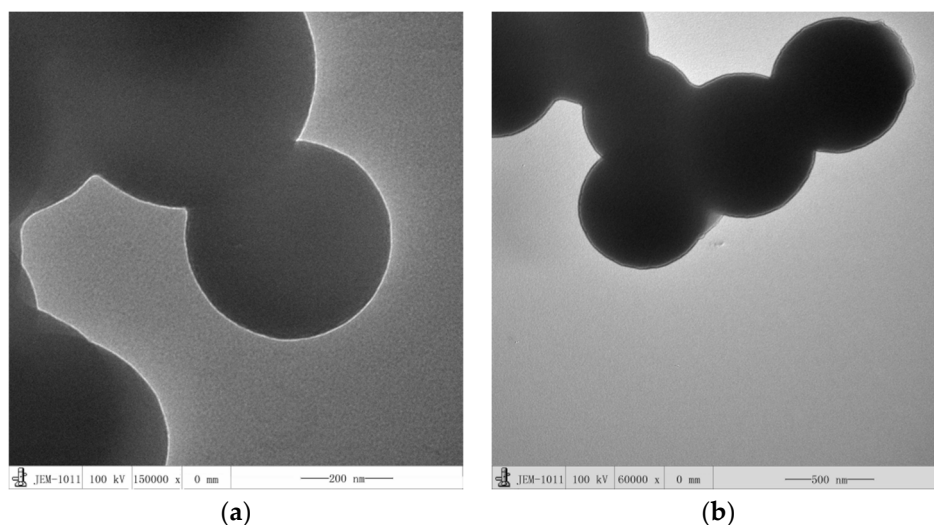


**Figure 3.** The transmission electron microscope (TEM) image of OCMSs (a) and FCMSs (b).

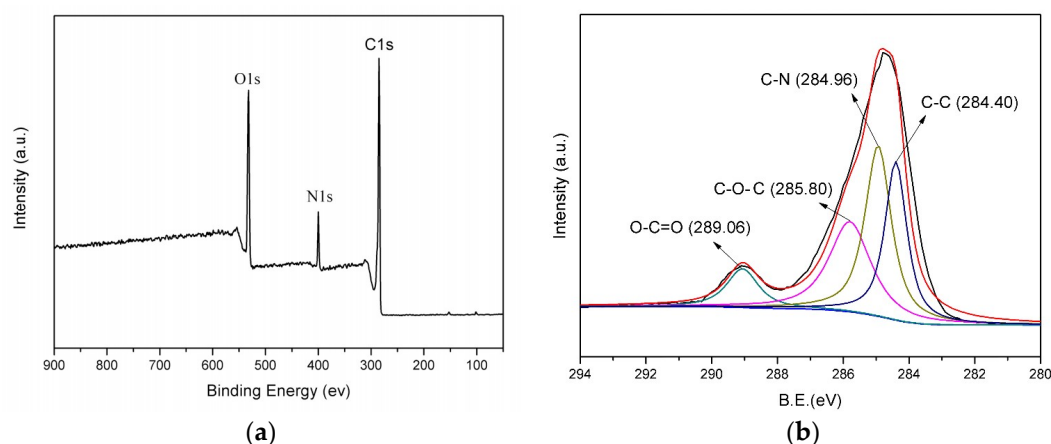


**Figure 4.** (a) The X-ray photoelectron spectroscopy (XPS) spectra of FCMSs; (b) The C1s spectra of FCMSs.

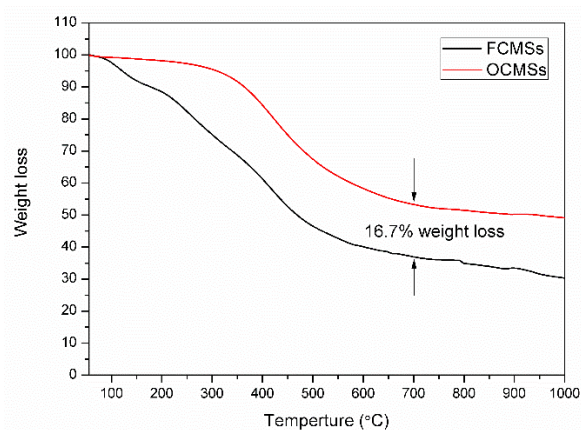


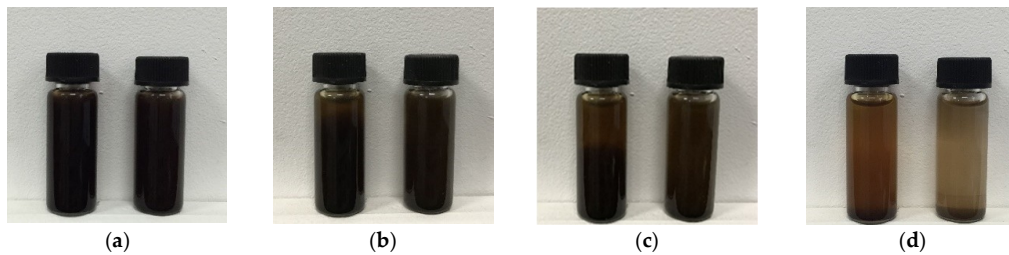
**Figure 5.** The TG spectra of FCMSs and OCMSs.

### 3.3. Study on the Dispersion of Carbon Microspheres in Solvent

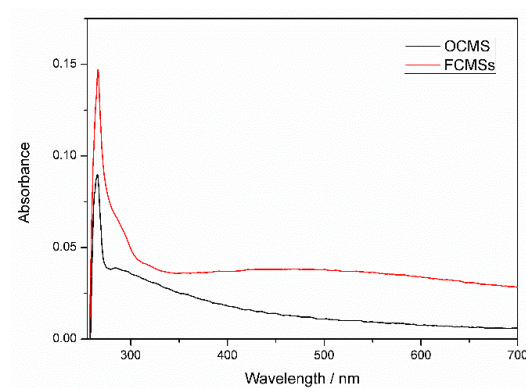
Since the organic modification of OCMSs was carried out in acetone, the same solvent was chosen to investigate the dispersity of carbon microspheres in solution during different time periods. Figure 6a showed the state of FCMSs and OCMSs after ultrasonic dispersion in acetone for 30 min. It could be seen that OCMSs and FCMSs had good dispersity in acetone. In Figure 6b, OCMSs showed obvious stratification after 2 h standing, while FCMSs still had good dispersity. As shown in Figure 6c, the stratification of OCMSs was further aggravated after 4 h of standing, and FCMSs began to appear slightly stratified. As shown in Figure 6d, after 18 h of standing, OCMSs and FCMSs were completely precipitated and the solution was separated into two phases. This indicated that the organic functional groups grafted on the surface of FCMSs had improved their ability to disperse in acetone to a certain extent. To further confirm the dispersity of OCMSs and FCMSs in acetone, the supernatant was analyzed by UV-Vis spectrometer after standing for 18 h (Figure 7). The strong peaks at 265 nm indicated that the absorbance of FCMSs was stronger than that of OCMSs, which suggested that the dispersity of FCMSs in acetone was better than that of OCMSs.

Figure 8 showed the dispersion state of FCMSs in different pH solution. Figure 9 showed the UV-Vis spectra of FCMSs in acidic, alkaline and neutral suspension. It could be seen from Figure 8 that FCMSs had good dispersity in solution of pH = 2 and pH = 12, and after 24 h both of the solution was uniformly precipitated. The dispersity in solution of pH = 4, pH = 7 and pH = 10 was low, and after 24 h, there was a significant agglomeration on the bottle wall. From Figure 9, it was clearly seen that the dispersity of FCMSs in different solution was in descending order followed by: pH = 12, pH = 2,

pH = 7, pH = 8 and pH = 6. The dispersivity of FCMSs in strong acid and alkali solution was better than that in neutral solution. And the dispersivity of FCMSs in neutral solution was better than that in weak acid and weak alkali solution.



**Figure 6.** The dispersion of FCMSs and OCMSs in acetone solution: (a) Initial state; (b) 2 h; (c) 4 h; (d) 18 h. The left side of each picture was OCMSs and the right one is FCMSs.



**Figure 7.** The UV-Vis spectra of FCMSs and OCMSs.

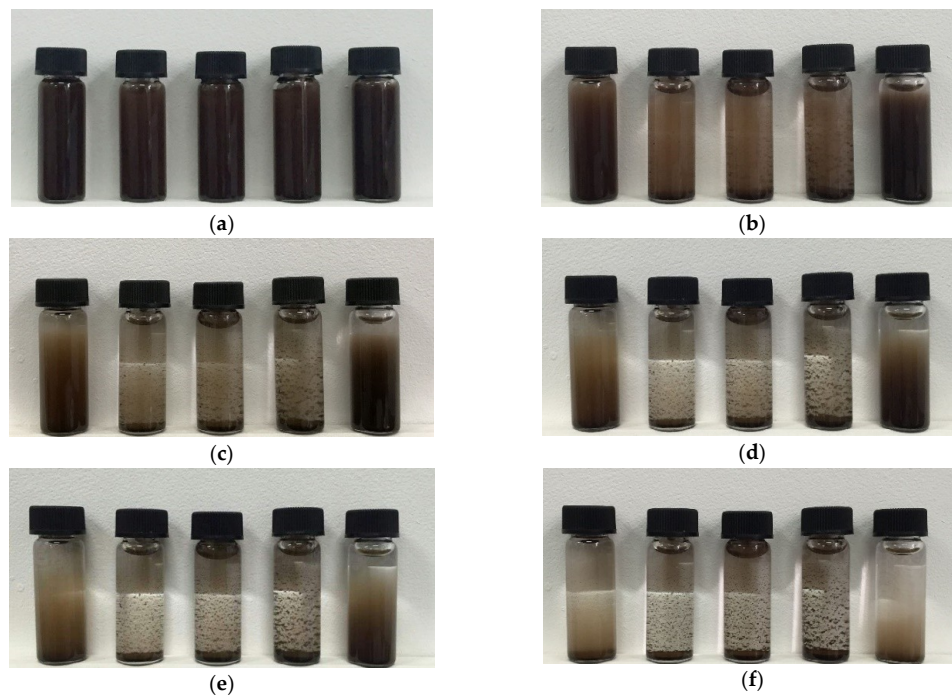


**Figure 8.** The dispersivity of FCMSs in the solutions with different pH. (a) Initial state; (b) 2 h; (c) 5 h; (d) 8 h; (e) 11 h; (f) 24 h. Images in each picture from left to right were the solution with the pH of 2, 6, 7, 8 and 12.

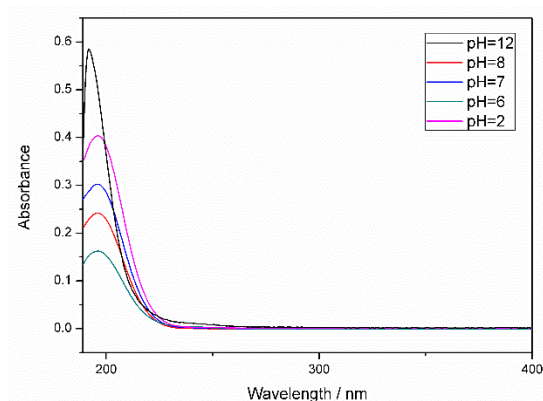


**Figure 9.** The UV-Vis spectra of FCMSs in acidic, alkaline and neutral suspensions.

#### 3.4. Performance of UV-Curable Coatings

Figure 10 showed the TGA and Differential thermal gravity (DTG) spectra of UV cured films. As can be seen from Figure 10, all samples had two weight loss stages. The comprehensive performance of UV-curable coatings was shown in Table 1. The first and second stage were the thermal decomposition of the soft segments in the PUA molecular chains and hard segments respectively. The first stage of the starting weight loss temperature ( $T_{5\%}$ ) was near 290 °C and the peak temperature of DTG ( $T_{max1}$ ) was near 338 °C, in which the  $T_{max1}$  of PUA/FCMSs-1 reached 343 °C. The corresponding temperature when the sample weight loss rate reached 50% ( $T_{50\%}$ ) was near 410 °C, and the peak temperature of DTG at the second stage ( $T_{max2}$ ) was near 417 °C. Compared with pure PUA, composites had better thermal stability as shown in Table 1. It could be seen that the TG curve of the UV-curable coating had good smoothness from Figure 10, which indicated that the UV-curable PUA molecular chains had good flowability and could disperse the heat in time. In addition, the addition of FCMSs or OCMS did not affect the movement of PUA molecular chains, while they were contributed to the dispersion of local heat. The addition of FCMS can increase the cross-linking density, which are also responsible for giving an improved thermal stability. Therefore, adding FCMSs or OCMs can help to improve the thermal performance of PUA. Moreover, compared to PUA, the pencil hardness also increased.

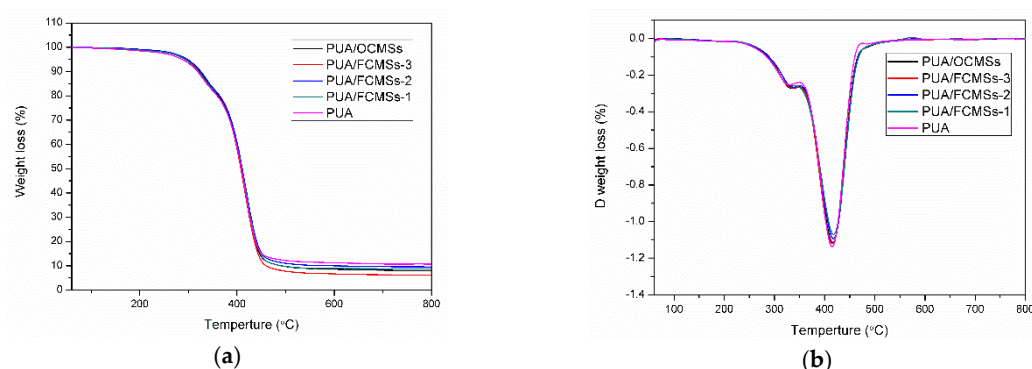


**Figure 10.** (a) The thermogravimetric analysis (TGA) spectra of UV cured films; (b) The Differential thermal gravity (DTG) spectra of UV-cured films.

**Table 1.** The comprehensive performances of UV-curable coatings.

Samples	$T_{5\%}$ (°C)	$T_{50\%}$ (°C)	$T_{\max 1}$ (°C)	$T_{\max 2}$ (°C)	GR (%)	WR (%)	WCA (°)	Pencil Hardness
PUA	285	409	329	415	94	52	72	H
PUA/FCMSs-1	293	410	343	418	99	30	73	2H
PUA/FCMSs-2	297	411	338	418	99	33	83	3H
PUA/FCMSs-3	294	408	338	415	98	38	106	4H
PUA/OCMSs	298	409	335	417	95	37	89	4H

Figure 11 showed the water contact angles of the UV-curable coatings. For PUA coatings, the gel rate (GR), water absorption (WA), water contact angle (WCA) and pencil hardness were 94%, 52%, 72° and H, respectively. After adding 1% OCMSs, the gel rate of the UV-curable coating was increased by 1%, while the water absorption was reduced to 37% and the water contact angle reached 89°. When FCMSs were introduced into the system, the gel rate and pencil hardness of UV-curable coatings were increased up to 99% and 4H, respectively. The water absorption was reduced to 30%–38%. At the same time, the water contact angle was improved and the hydrophilic property was reduced. Especially for PUA/FCMSs-3, water contact angle was increased to 106° and this showed significant hydrophobicity. The obvious increase in gel rate, when FCMSs were added into PUA, indicated that the active double bonds on the surface of FCMSs were involved in the UV curing process of matrix resin PUA. The results of Table 1 also showed that both FCMSs and OCMSs had the effect to enhance the pencil hardness of PUA. With the increase of FCMSs, the pencil hardness distinctly improved. The reason for this may be due to both the increase of C–O–C inorganic network and cross-linking density by the addition of FCMSs, which improves the hardness and corrosion resistance.

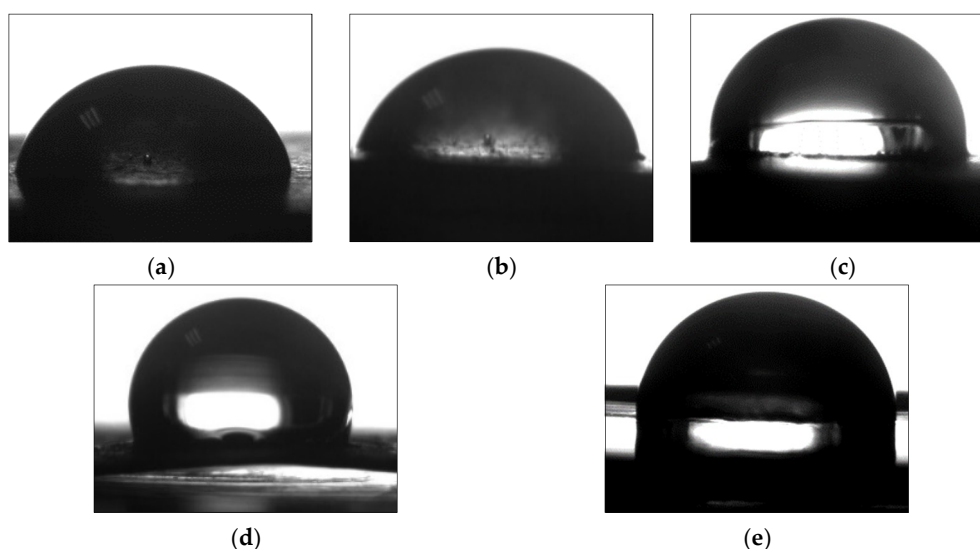


**Figure 11.** The water contact angles of UV curing films: (a) PUA; (b) PUA/FCMSs-1; (c) PUA/FCMSs-2; (d) PUA/FCMSs-3; (e) PUA/OCMSs.

The XRD images of UV curing film was shown in Figure 12. Compared with pure PUA, all the PUA composites had a proliferation of diffraction peak near 20°. These peaks were attributed to the short distance arrangement of the amorphous segment of the PUA molecule chains and the uniform three-dimensional network structure formed in the PUA molecule chains. OCMSs and FCMSs also had similar steamed points near 20°, which corresponded to the (002) plane of graphite [9,13]. With the increase of FCMSs content, the peak width and peak height of the diffraction peak of UV-curable films increased gradually. These results showed that there was a strong interaction between FCMSs and matrix resin, and with the increase of FCMSs content, the interaction between them gradually

increased. The XRD spectra of PUA/OCMSs and PUA/FCMSs-3 showed that both of them had the same width of peak near  $20^\circ$ , while the height of the former was lower than the latter. This indicated that the interaction between OCMSs and PUA was smaller than that between the FCMSs and PUA when the filler quality was at the same level. These phenomena further indicated that FCMSs and PUA molecular chains were connected in the form of chemical bonds.

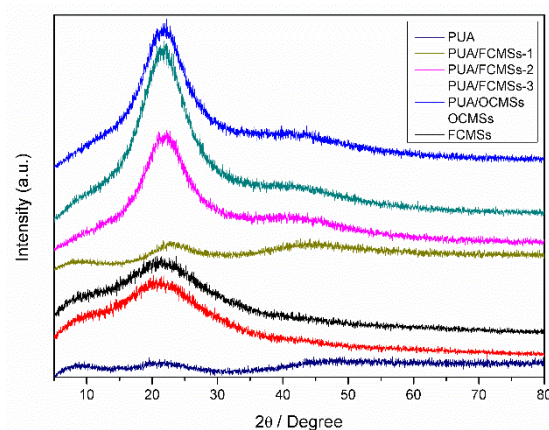


**Figure 12.** X-ray diffraction images of OCMSs and FCMSs.

CMSs had a very smooth surface and there were some interconnections between carbon spheres. This may be because that the hydrothermal process led to burst nucleation and durative polycondensation of glucose molecules, finally developing irregular and crosslinked carbonaceous clusters [16]. After being oxidized, the surface of OCMSs became relatively rough. There were some fractures between the crosslinked carbonaceous clusters. Figure 13c,d contained the cross-sectional scan of PUA/FCMSs-3 sample. It could be seen from the figure that FCMSs had good dispersity in PUA matrix. The phenomenon of crack termination was clearly observed around FCMSs particles which indicated that the interfacial force between PUA and FCMSs was very strong. Figure 13e,f showed cross-sectional scans of the PUA/OCMSs samples, in which obvious fracture micro-holes could be found and OCMSs had low dispersity in PUA matrix. The micro-holes showed that the interfacial force between PUA and OCMSs was very poor. In composite materials, the difficulty of crack propagation along the interface can have a great influence on the mechanical properties of the material. Potentiation of FCMSs was better than that of OCMSs and this can be explained in the following ways: first, there was organic matter grafted on the surface of FCMSs so that it had a better dispersion in the PUA prepolymer. Second, after the surface of the ball was modified, the carbon-carbon double bond (C=C) was introduced to its surface, and under UV irradiation, the double bonds on the surface and in the PUA prepolymer were condensed together to enhance the interface interaction.

The results of Nyquist plots and Bode spectrum were shown in Figures 14 and 15, respectively. It can be seen from Figure 14 that, with the increase of FCMSs content, the capacitive arc radius of the PUA/FCMSs coatings increased gradually, and they were all larger than that of pure PUA coatings, while the capacitive arc radius of the PUA/OCMSs coatings was smaller than that of pure PUA coatings. The results of Figure 15 indicated that, in low frequency area, the impedance modulus value of PUA/FCMSs coatings increased gradually when the content of FCMSs increased from 0% to 1%. When the content of FCMSs was 1%, the resistance modulus of the coatings in the low frequency zone was as high as  $3.5 \times 10^4 \Omega \cdot \text{cm}^2$ . However, the impedance modulus value of PUA/OCMSs coatings was smaller than that of pure PUA in low frequency area. The results of Bode spectrum were consistent with the results of Nyquist plots.

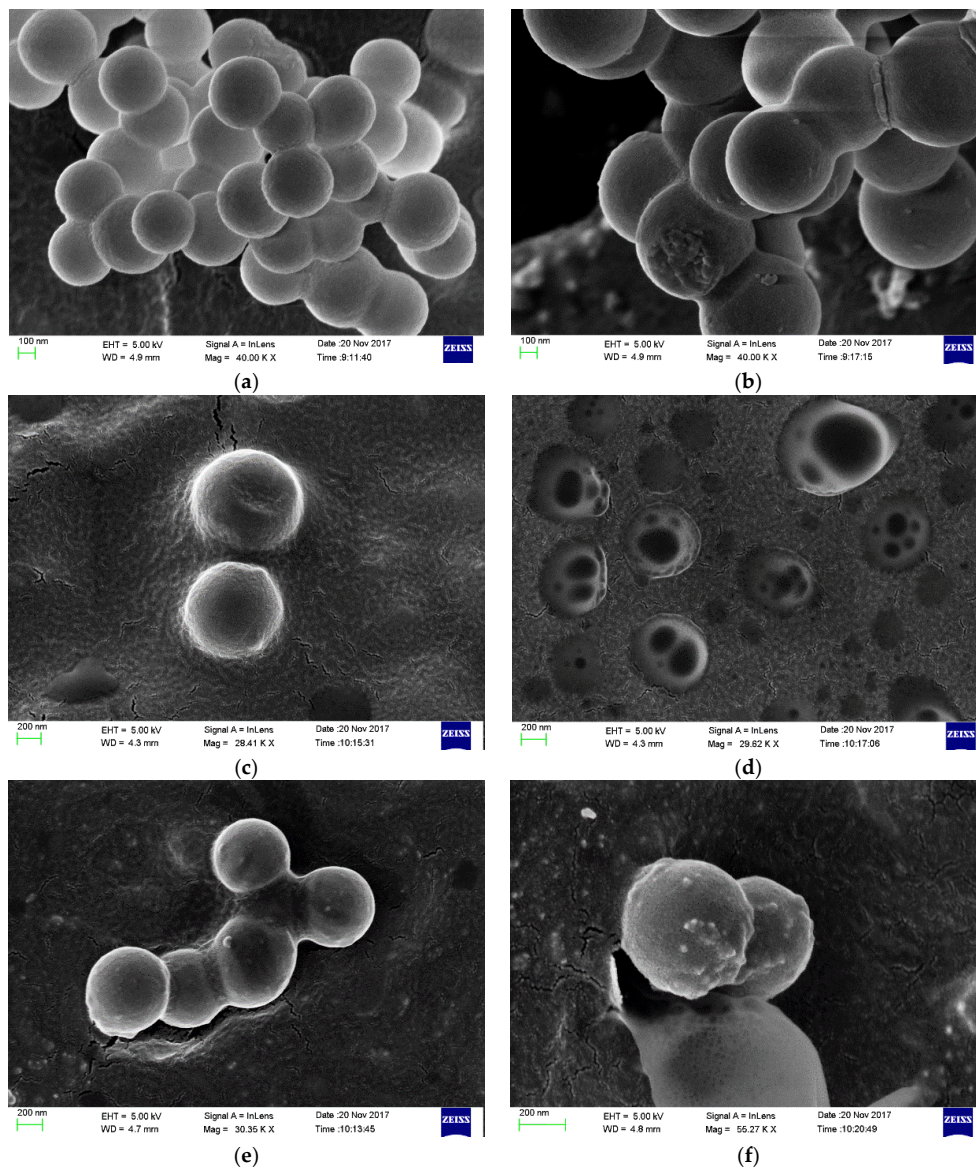


**Figure 13.** The SEM image of section of samples. (a) CMSs; (b) OCMSs; (c) PUA/FCMSs-3; (d) PUA/FCMSs-3; (e) PUA/OCMSs; (f) PUA/OCMSs.

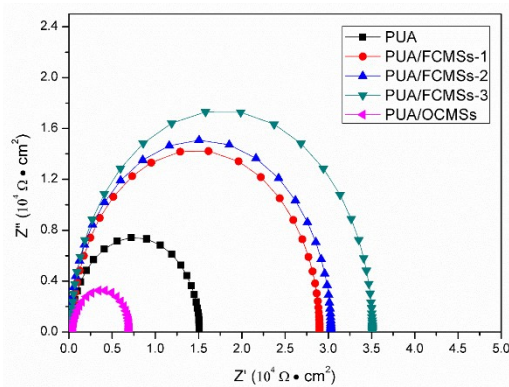


**Figure 14.** Nyquist plots of UV-curable polyurethane composite coatings.

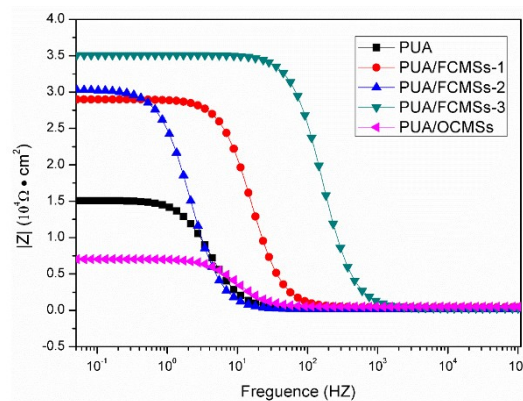


Figure 15. Bode spectrum of UV-curable polyurethane composite coatings.

The polarization curves of UV-curable coatings were shown in Figure 16. The electrochemical characteristic parameters of the coatings fitted by Tafel (traditional method) were shown in Table 2. As can be seen from Table 2, with the increase of FCMSs content, the corrosion current ( $I_{\text{corr}}$ ) and the corrosion rate ( $V_{\text{corr}}$ ) of PUA/FCMSs coatings decreased gradually. And those parameters were all lower than those of pure PUA. The natural corrosion potential ( $E_0$ ) of PUA/FCMSs coatings had positive shifts compared with pure PUA. When the content of FCMSs and OCMSs were all 1%, the corrosion current of PUA/FCMSs was lower than that of PUA/OCMSs.

This phenomenon indicated that PUA/FCMSs coatings had better corrosion resistance and can effectively prevent ions to penetrate coatings in the corrosive medium. The reason was that, compared with OCMSs, FCMSs had a better dispersity in PUA system. FCMSs had good filling effect and crosslinking effect, which resulted in an increase for the coatings' gel rate and a decrease for the content of micro-holes. These eventually effectively prevented the corrosive ions to go through the coatings. OCMSs were easy to reunite in PUA system which made the internal structure of PUA/OCMSs heterogeneous, which facilitated the corrosive ions to go through the coatings.

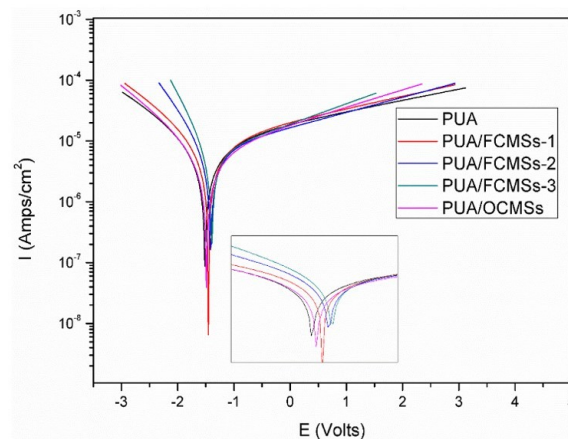


Figure 16. The polarization curve of UV-curable polyurethane composite coatings.

Table 2. Electrochemical characteristic parameters of UV-curable polyurethane composite coatings.

Samples	$I_{\text{corr}}$ (Amp $\text{cm}^{-2}$ )	$E_0$ (V)	$V_{\text{corr}}$ (mm/a)
PUA	$1.0550 \times 10^{-5}$	-1.5143	0.124
PUA/FCMSs-1	$1.0340 \times 10^{-5}$	-1.4525	0.106
PUA/FCMSs-2	$7.4238 \times 10^{-6}$	-1.4139	0.087
PUA/FCMSs-3	$6.5122 \times 10^{-6}$	-1.3959	0.076
PUA/OCMSs	$6.9574 \times 10^{-6}$	-1.4873	0.082

#### 4. Conclusions

In conclusion, the modification on the surface of carbon microspheres by organic groups was successful and the active double bond was introduced on the surface of FCMSs. FCMSs had good dispersity in both acetone and alkaline solution of pH = 12. The double bond of FCMSs surface was involved in the UV curing process, which improved the gel rate, water contact angle, mechanical property, thermal stability, and corrosion resistance of PUA resin. This PUA can be used in many areas. Applying this coating on the housing can effectively increase the corrosion resistance of the housing. It also can increase the hydrophobicity of the housing. The colour of this new PUA coating is light brown and it can be changed by adding pigments. However, after adding the colour, its transparency may be affected. To sum up, this UV coating has many advantages, which may attract people's attention more and more.

**Author Contributions:** Conceptualization, X.L. and J.W.; Methodology, X.L., H.L. (Houbin Li), C.H. and J.W.; Software, J.W.; Validation, J.W. and C.F.; Formal Analysis, J.W., C.F., H.L. (Huijie Li) and F.D.; Investigation, J.W. and C.F.; Resources, X.L.; Data Curation, X.L.; Writing-Original Draft Preparation, J.W.; Writing-Review & Editing, J.W., C.F. and X.L.; Visualization, J.W. and C.F.; Supervision, X.L.; Project Administration, X.L.; Funding Acquisition, X.L.

**Funding:** This research was funded by the National Natural Science Foundation of China (No. 51776143) and Fundamental Research Funds for Central Universities (No. 2042018kf0238).

**Acknowledgments:** The materials of this work were provided by the Integration Innovation Centre of Hubei Aerospace Power and Material Technology Military and Civil. The TEM and SEM photographs were characterized by Changchun Institute of Applied Chemistry Chinese Academy of Sciences, Test Centre of Wuhan University, respectively. We gratefully acknowledge Xu Qiyang for his contribution to diagram analysis.

**Conflicts of Interest:** The authors declare no conflict of interest.

#### References

1. Yan, X.X.; Qian, X.Y.; Lu, R.; Miyakoshi, T. Synergistic Effect of Addition of Fillers on Properties of Interior Waterborne UV-Curing Wood Coatings. *Coatings* **2018**, *8*, 9. [[CrossRef](#)]
2. Yang, Z.L.; Douglas, A.W.; Charles, E.H.; Pu, H.T.; Yuan, J.J.; Wan, D.C.; Liu, Y.S. Newly UV-curable polyurethane coatings prepared by multifunctional thiol- and ene-terminated polyurethane aqueous dispersions mixtures: Preparation and characterization. *Polymer* **2009**, *7*, 1717–1722. [[CrossRef](#)]
3. Dong, F.; Maganty, S.; Meschter, S.J.; Cho, J. Effects of curing conditions on structural evolution and mechanical properties of UV-curable polyurethane acrylate coatings. *Prog. Org. Coat.* **2018**, *114*, 58–67. [[CrossRef](#)]
4. Zhang, T.; Wu, W.J.; Wang, X.J.; Mu, Y.P. Effect of average functionality on properties of UV-curable waterborne polyurethane-acrylate. *Prog. Org. Coat.* **2010**, *68*, 201–207. [[CrossRef](#)]
5. Li, Y.Y.; Yang, Z.Z.; Qiu, H.X.; Zheng, Q.B.; Li, J.; Yang, J.H. Self-aligned graphene as anticorrosive barrier in waterborne polyurethane composite coatings. *J. Mater. Chem. A* **2014**, *2*, 14139–14145. [[CrossRef](#)]
6. Tsai, P.Y.; Chen, T.E.; Lee, Y.L. Development and Characterization of Anticorrosion and Antifriction Properties for High Performance Polyurethane/Graphene Composite Coatings. *Coatings* **2018**, *8*, 250. [[CrossRef](#)]
7. Estekhradj, S.A.Z.; Amiri, S. Synthesis and Characterization of Anti-fungus; Anti-corrosion and Self-cleaning Hybrid Nanocomposite Coatings Based on Sol–Gel Process. *J. Inorg. Organomet. Polym.* **2017**, *27*, 883–891. [[CrossRef](#)]
8. Ma, I.A.W.; ShRamesh, A.K.; Vengadaesvaran, B.; Ramesh, S.; Arof, A.K. Anticorrosion Properties of Epoxy-Nanochitosan Nanocomposite Coating. *Bioresources* **2017**, *12*, 2912–2929. [[CrossRef](#)]
9. Atta, A.M.; El-Saeed, A.M.; Al-Lohedan, H.A.; Wahby, M. Effect of Montmorillonite Nanogel Composite Fillers on the Protection Performance of Epoxy Coatings on Steel Pipelines. *Molecules* **2017**, *22*, 905. [[CrossRef](#)] [[PubMed](#)]
10. Purcar, V.; Şomoghi, R.; Niţu, S.G.; Nicolae, C.A.; Alexandrescu, E.; Gîfu, I.C.; Gabor, A.R.; Stroescu, H.; Ianchiş, R.; Căprărescu, S.; et al. The Effect of Different Coupling Agents on Nano-ZnO Materials Obtained via the Sol–Gel Process. *Nanomaterials* **2017**, *7*, 439. [[CrossRef](#)] [[PubMed](#)]

11. Wang, N.; Diao, X.L.; Zhang, J.; Kang, P. Corrosion Resistance of Waterborne Epoxy Coatings by Incorporation of Dopamine Treated Mesoporous-TiO<sub>2</sub> Particles. *Coatings* **2018**, *8*, 209. [[CrossRef](#)]
12. Yan, T.N.; Xu, J.L.; Chu, Z.Y.; Liu, E.H.; Yang, L.; Wang, C.H. Hydrothermal Synthesis and Electrochemical Properties of N-doped Activated Carbon Microspheres. *Int. J. Electrochem. Sci.* **2017**, 6118–6128. [[CrossRef](#)]
13. Ma, A.L.; Wang, X.M.; Li, T.B.; Liu, X.G.; Xu, B.S. Characteristics of carbon microspheres and study on its adsorption isotherms. *Mater. Sci. Eng. A* **2007**, *443*, 54–59. [[CrossRef](#)]
14. Sun, B.F.; Li, H.L.; Li, X.Y.; Liu, X.W.; Zhang, C.H.; Xu, H.Y.; Zhao, X.S. Degradation of Organic Dyes over Fenton-like Cu<sub>2</sub>O-Cu/C Catalyst. *Ind. Eng. Chem. Res.* **2018**, *57*, 14011–14021. [[CrossRef](#)]
15. Sun, X.M.; Li, Y.D. Colloidal carbon spheres and their core/shell structures with noble-metal nanoparticles. *Angew. Chem. Int. Ed.* **2004**, *43*, 597–601. [[CrossRef](#)] [[PubMed](#)]
16. Zheng, M.T.; Liu, Y.L.; Xiao, Y.; Zhu, Y.; Guan, Q.; Yuan, D.S.; Zhang, J.X. An Easy Catalyst-Free Hydrothermal Method to Prepare Monodisperse Carbon Microspheres on a Large Scale. *J. Phys. Chem. C.* **2009**, *113*, 8455–8459. [[CrossRef](#)]
17. Ryu, G.; Suh, Y.W.; Dong, J.S.; Dong, J.A. Hydrothermal preparation of carbon microspheres from mono-saccharides and phenolic compound. *Carbon* **2010**, *48*, 1990–1998. [[CrossRef](#)]
18. Kumar, S.; Kothari, U.; Kong, L.Z.; Lee, Y.Y.; Gupta, R.B. Hydrothermal pretreatment of switchgrass and corn stover for production of ethanol and carbon microspheres. *Biomass Bioenerg.* **2011**, *35*, 956–968. [[CrossRef](#)]
19. Gong, Y.T.; Xie, L.; Li, H.; Wang, Y. Sustainable and scalable production of monodisperse and highly uniform colloidal carbonaceous spheres using sodium polyacrylate as the dispersant. *Chem. Commun.* **2014**, *50*, 12633–12636. [[CrossRef](#)] [[PubMed](#)]
20. Gan, L.; Geng, A.B.; Xu, L.J.; Chen, M.J.; Wang, L.C.; Liu, J.; Han, S.G.; Mei, C.T.; Zhong, Q. The fabrication of bio-renewable and recyclable cellulose based carbon microspheres incorporated by CoFe<sub>2</sub>O<sub>4</sub> and the photocatalytic properties. *J. Cleaner Prod.* **2018**, *196*, 594–603. [[CrossRef](#)]
21. Titirici, M.M.; Antonietti, M. Chemistry and materials options of sustainable carbon materials made by hydrothermal carbonization. *Chem. Soc. Rev.* **2010**, *39*, 103–116. [[CrossRef](#)] [[PubMed](#)]
22. Wen, J.J.; Li, H.J.; Liu, X.H.; Huang, C.; Li, H.B. Organic modification of silica and its application in polyurethane acrylate coatings. *Packag. J.* **2017**, *9*, 42–497. (In Chinese)
23. Wen, J.J.; Wang, D.; Liu, X.H.; Huang, C.; Li, H.B. Synthesis and properties of UV-curable polyurethane acrylate coatings. *Packag. J.* **2017**, *9*, 65–71. (In Chinese) [[CrossRef](#)]
24. Zhang, Q.Y.; Huang, C.; Wang, H.X.; Hu, M.J.; Li, H.B.; Liu, X.H. UV-curable coating crosslinked by a novel hyperbranched polyurethane acrylate with excellent mechanical properties and hardness. *RSC Adv.* **2016**, *6*, 107942–107950. [[CrossRef](#)]
25. Lv, C.H.; Hu, L.; Yang, Y.; Li, H.B.; Huang, C.; Liu, X.H. Waterborne UV-curable polyurethane acrylate/silica nanocomposites for thermochromic coatings. *RSC Adv.* **2015**, *5*, 25730–25737. [[CrossRef](#)]
26. Liu, R.; Zhang, X.P.; Zhu, J.J.; Liu, X.Y.; Wang, Z.; Yan, J.L. UV-Curable Coatings from Multiarmed Cardanol-Based Acrylate Oligomers. *ACS Sustain. Chem. Eng.* **2015**, *3*, 1313–1320. [[CrossRef](#)]

